

# Latent-Reframe: Enabling Camera Control for Video Diffusion Model without Training

Zhenghong Zhou\*, Jie An\*, Jiebo Luo  
University of Rochester

zzhou72@ur.rochester.edu, {jan6, jluo}@cs.rochester.edu

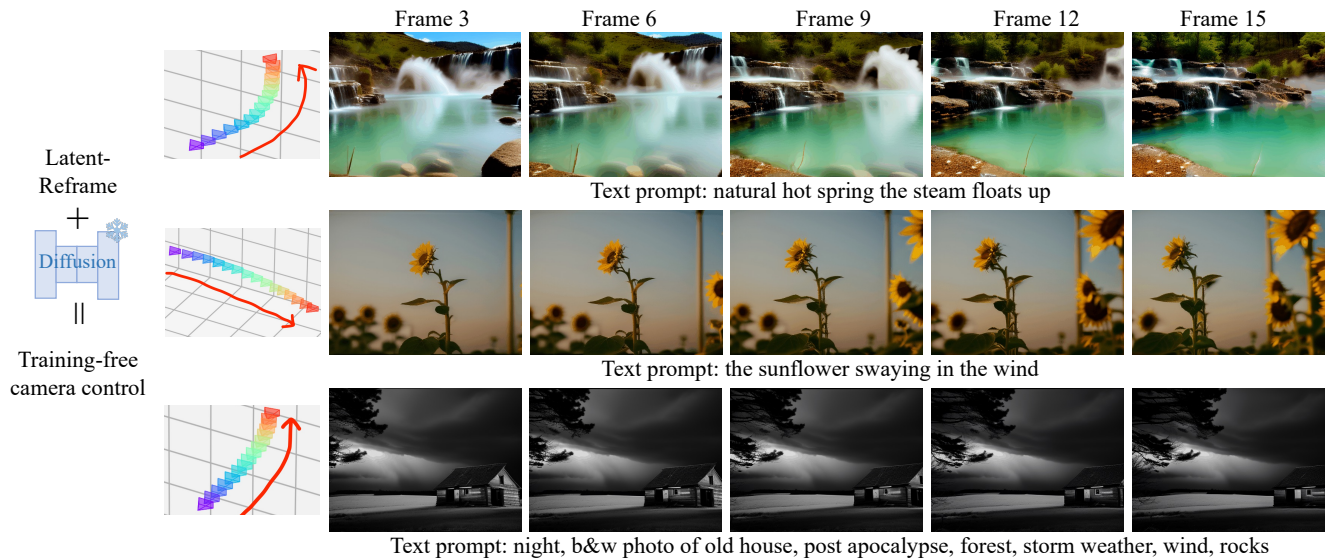


Figure 1. The proposed Latent-Reframe enables a text-to-video diffusion model to generate high-quality videos that accurately follow both the text prompt and a specified camera trajectory, all without requiring additional training.

## Abstract

Precise camera pose control is crucial for video generation with diffusion models. Existing methods require fine-tuning with additional datasets containing paired videos and camera pose annotations, which are both data-intensive and computationally costly, and can disrupt the pre-trained model’s distribution. We introduce Latent-Reframe, which enables camera control in a pre-trained video diffusion model without fine-tuning. Unlike existing methods, Latent-Reframe operates during the sampling stage, maintaining efficiency while preserving the original model distribution. Our approach reframes the latent code of video frames to align with the input camera trajectory through time-aware point clouds. Latent code inpainting and harmonization then refine the model’s latent space, ensuring high-quality video generation. Experimental results demonstrate that

*Latent-Reframe achieves comparable or superior camera control precision and video quality to training-based methods, without the need for fine-tuning on additional datasets.*

## 1. Introduction

Generating a video that follows a user-defined camera trajectory is a key task for controllable video generation. Existing methods, such as CameraCtrl [11] and MotionCtrl [40], inject camera control into a pre-trained video diffusion model by fine-tuning it with an additional dataset containing paired videos and camera trajectories.

While these methods demonstrate good performance, they face two key challenges: 1) Fine-tuning requires an extra dataset annotated with camera trajectories, which is labor-intensive to collect and computationally expensive in training, even with techniques like Low-Rank Adaptation

\*Equal contribution

(LoRA) [17]. 2) Fine-tuning can disrupt the learned distribution of the pre-trained video diffusion model, potentially degrading the quality of the generated videos if the fine-tuning dataset is of lower quality. This raises an important question: Can camera control be injected into a pre-trained video diffusion model without encountering these issues?

Building on insights from image editing research [29, 49] showing that pre-trained diffusion models can accommodate latent code manipulation, we introduce Latent-Reframe, a sampling-stage method that enables camera control in video diffusion models without fine-tuning. Midway through the denoising process, our method performs two key steps: latent code reframing to align the video latent with the target camera pose and latent space rehabilitation to inpaint and harmonize the latent code.

Given a pre-trained video diffusion model, such as AnimateDiff [9], we use MonSt3R [48] to extract per-frame 3D point clouds and corresponding camera poses from partially denoised latent codes. We then adjust each frame’s camera pose to match the user-defined target positions and reproject the time-aware 3D point clouds to video frames based on these adjusted poses, creating frames that follow the desired camera trajectory. These reframed frames are then converted to latent codes via the VAE encoder, ready for the remaining denoising steps.

The latent code reframing process can create blank regions in the video’s latent code due to occlusion. To address this, we propose a latent space rehabilitation process to inpaint these regions and harmonize the latent code. Specifically, we add noise to both the warped latent codes and blank regions, then denoise to fill in the missing content. Inspired by FIFO-Diffusion [20], we apply lighter noise to the warped latent codes, enabling the blank regions to incorporate content from the reframed area, which improves video content preservation. After rehabilitation, we complete the remaining denoising steps, producing a video aligned with the desired camera trajectory.

We compare Latent-Reframe with state-of-the-art, training-based baselines, including CameraCtrl [11] and MotionCtrl [40], using 10 prompts and 80 camera trajectories. Experimental results show that our method, without fine-tuning, enables a pre-trained video diffusion model to achieve comparable or even superior camera control precision. Additionally, videos generated by our method demonstrate higher quality, as measured by FID [12] and FVD [35] scores, indicating a stronger capacity to preserve the video generation quality of the pre-trained model.

This work contributes to the field by introducing Latent-Reframe, which leverages latent reframing through 3D point cloud remapping, enabling camera control in a pre-trained video diffusion model without fine-tuning. Results show that Latent-Reframe produces videos with precise camera pose trajectories and superior quality compared

to training-based methods, highlighting the potential of 3D information to enhance 2D video generation.

## 2. Related work

**Camera Control for Video Diffusion Model.** Recent advancements in diffusion models [2, 3, 13, 18, 25, 32, 34] have enabled the generation of high-quality videos. To make video diffusion models [1, 4–6, 6, 8, 10, 14, 15, 30, 36, 37, 39, 41, 45] follow a camera pose trajectory, two types of approaches are commonly used.

The first approach is implicit camera pose control, where poses are embedded and injected into the UNet denoising network. Methods like MotionCtrl [40], CameraCtrl [11], CamCo [42], and Direct-a-Video [43] fall under this category. However, these methods require extensive training on large, high-quality datasets, demanding significant computational and data resources.

The second approach uses explicit pose control, where a point cloud is extracted, and the pose is used to render frames before denoising. Latent-Reframe aligns with this category, similar to CamTrol [16] and ReCapture [47]. Unlike these methods, which rely on static point cloud rendering and are limited to image-to-video generation, Latent-Reframe employs time-aware point clouds, enabling both text-to-video and image-to-video generation. Empirically, time-aware point clouds outperform static ones in capturing complex video dynamics, making Latent-Reframe more versatile and effective for diverse tasks.

**3D Reconstruction and Novel View Synthesis.** 3D reconstruction and novel view synthesis aim at learning scene details from sparse input views [19, 24]. DUST3R [38] advances 3D reconstruction from sparse inputs by enabling scene point cloud reconstruction and camera pose estimation from just two images, while MonST3R [48] further improves results in dynamic reconstruction. Other methods, such as InstanSplat [7], NoPoSplat [44], and Splatt3R [31], support 3D Gaussian Splatting reconstruction from extremely sparse views. Integrated with video diffusion models, tools like ViewCrafter [46] and ReconX [22] have achieved enhanced 3D and even 4D reconstruction. These advances demonstrate that 3D reconstruction models can infer dense scene information from sparse data, providing strong potential for generative tasks. However, current methods typically require extensive training, especially with video diffusion models, which are computationally intensive. This paper proposes a method to enhance generative model quality and control using 3D reconstruction without additional training.

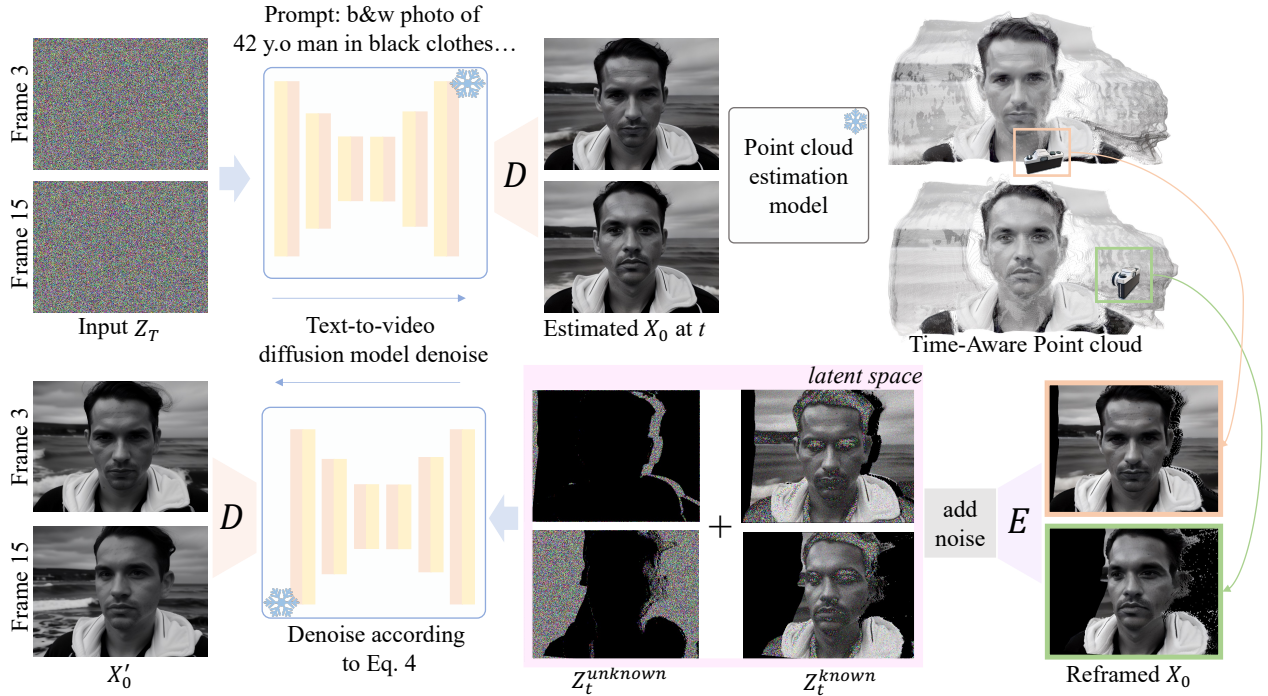


Figure 2. **Overview of the proposed Latent-Reframe.** In the middle of the denoising process of a pre-trained video diffusion model, we first extract time-aware 3D point cloud via a point cloud estimation model, which takes  $x_0$  estimated by the halfway denoised latent code as the input. Next we reframe  $x_0$  according to the target camera pose and the per-frame point cloud. Then we use the proposed latent space rehabilitation approach to inpaint the blank region due to occlusion and harmonize the latent code.  $x'_0$  is the reframed video after finishing the remaining denoising steps, which follows the target camera pose trajectory.

### 3. Method

To enable camera control in a video diffusion model through latent code manipulation without training, we face two key challenges: 1) Extracting precise camera poses from partially denoised latent codes and reframing the latent codes to align with the target camera pose trajectory. 2) Inpainting and harmonizing the reframed video latents to preserve the quality of the generated videos.

This section details our solutions to these challenges. In Sec.3.1, we outline the preliminaries of video diffusion models. Sec.3.2 explains our approach to manipulating latent codes during denoising to align videos with the desired camera trajectory. Sec. 3.3 describes how we rehabilitate the manipulated latent codes to maintain video quality. Fig. 2 and Alg. 1 provide an overview and a pseudo-code of the proposed method, respectively.

#### 3.1. Preliminary of Video Diffusion Model

A video diffusion model maps the training video distribution to a Gaussian noise distribution through a forward and backward process. The forward process adds noise to the video, while the backward process iteratively recovers a

clean video from random Gaussian noise. For latent video diffusion models, the training data consists of latent codes  $z_0 = \{z_0^0, z_0^1, \dots, z_0^F\}$  where  $z_0^n$  represents the latent code of the  $n^{\text{th}}$  video frame, and  $F$  is the number of frames in a video. During the forward process, noise is added to  $z_0$  as follows:

$$z_t = \sqrt{\bar{\alpha}_t} z_0 + \sqrt{1 - \bar{\alpha}_t} \epsilon, \quad \epsilon \sim \mathcal{N}(\mathbf{0}, \mathbf{I}) \quad (1)$$

where  $z_t$  is the noisy latent code at diffusion step  $t$ .  $\alpha_t$  and  $\bar{\alpha}_t$  are predefined constants by diffusion model. Eq. 1 allows recovery of the clean latent code  $z_0$  from partially denoised  $z_t$ , enabling the extraction of 3D point clouds and camera poses from halfway-denoised video latents (see Sec. 3.2 for details). The backward process takes a noisy latent  $z_t$  and produces the one-step denoised latent  $z_{t-1}$ . In this work, we use DDIM [33] sampler for the backward process.

The training objective of a video diffusion model is

$$\mathcal{L} = \mathbb{E}_{z_0, \epsilon, t} \left[ \|\epsilon - \epsilon_\theta(z_t, t, c)\|_2^2 \right], \quad (2)$$

where  $c$  is the optional conditions such as text embedding for text-to-video generation.  $\theta$  denotes the network archi-

texture (e.g., UNet [28] and DiT [26]), which captures spatial and temporal information to predict the added noise  $\epsilon$ .

### 3.2. Latent Reframing

We manipulate the latent code midway through the denoising process to ensure the generated video follows the specified camera pose trajectory. Starting from random noise at diffusion step  $T$ , when the diffusion model reaches a chosen denoising step  $t$ , we first derive an approximate  $z_0$  from  $z_t$  using Eq. 1 and then reconstruct the pixel-space video  $x_0$  based on this estimate of  $z_0$ . Next, we use MonST3R [48] to transform the 2D video into a sequence of time-aware 3D point clouds, where each point cloud corresponds to one video frame.

Notably, MonST3R requires image pairs as input, while the video contains 16 frames. Inferring each pair sequentially would lead to scale misalignment in point maps, necessitating a global alignment.

Following DUST3R [38], we construct a connectivity graph  $G(V, \mathcal{E})$ , where the 16 images form the vertices  $V$ , and each edge  $e = (n, m) \in \mathcal{E}$  represents an image pair  $(I_n, I_m)$  for model processing. To optimize computation, we build this graph using a sliding window approach, pairing images within each window. For example, with a window size of 3, we generate 6 image pairs, sliding the window until all frames are processed.

Our objective is to obtain globally aligned point maps for each frame in a common coordinate system, denoted as  $P_n \in \mathbb{R}^{W \times H \times 3}$  for all images  $n = 1, \dots, 16$ . Each image pair in the connectivity graph, when processed by MonST3R, produces a pair of point clouds. These point clouds can be mapped to the coordinate system of the globally aligned point maps by applying a scaling factor  $s$  and a pose transformation  $\tau \in \mathbb{R}^{3 \times 4}$ . We aim for these transformed point clouds to align with the globally aligned points. To achieve this, the globally aligned point maps  $P$ , scale  $s$ , and pose  $\tau$  are defined as learnable parameters, framing the task as an optimization problem for backpropagation. The objective function is:

$$P^* = \arg \min_{P, \tau, s} \sum_{e \in \mathcal{E}} \sum_{v \in e} \sum_{i=1}^{HW} C_i^{v,e} \|P_i^v - s_e \tau_e Q_i^{v,e}\|, \quad (3)$$

where  $C_i^{v,e}$  and  $Q_i^{v,e}$  represent the confidence score and point map, respectively, for the  $i$ -th pixel in image  $v$  on edge  $e$ . Here,  $H$  and  $W$  denote the height and width of frames.

Upon completion of the optimization, we obtain the point maps and corresponding poses for the 16 video frames in a unified coordinate system. Subsequently, we perform camera pose shifting to determine the target new poses for the image sequence. A series of poses from RealEstate10K [50] is utilized to compute the target poses. Initially, we process these poses by calculating the relative

pose, which involves determining the changes in pose relative to the first frame. After this, we apply normalization and scale adjustment. Finally, these processed poses are multiplied by the original poses of 16 frames, resulting in the target new poses for video frames.

Besides lifting each video frame into a time-aware 3D point cloud, one can alternatively reconstruct a global point cloud with all video frames [16], we empirically find that our time-aware point cloud results in fewer artifacts and better video quality when performing latent reframing. Please refer to Sec.4.3 for more details.

### 3.3. Latent Rehabilitation

Due to the presence of occlusions, the reframed video frames  $x'_t$  and their latent codes  $z'_t$  subjected to camera pose shifting often exhibit blank regions, resulting in reduced image quality. To address this, we propose a simple yet effective method to rehabilitate these occluded regions without using external models.

**Latent Code inpainting.** Inspired by RePaint [23], we use the video diffusion model itself to inpaint blank regions in the video latent code. After obtaining the reframed video latent code  $z'_t$  at the  $t$ -th denoising step, rather than proceeding with further denoising, we reintroduce noise to  $z'_t$ .

Specifically, we create a mask  $m$  to identify occluded regions lacking valid pixel values by detecting points unrendered by the time-aware point cloud. Random Gaussian noise is added to the masked regions, reverting them to the initial state of the denoising process at time step  $T$ . Noise is also added to the unmasked regions; however, during the follow-up denoising step, only the masked regions are updated, while the unmasked regions are directly computed with Eq. 1 using  $z'_0$ . This iterative process continues until the  $t$ -th denoising step, by which point the noise levels in both occluded and non-occluded regions become aligned.

$$\begin{aligned} z_{t-1}^{\text{known}} &\sim \sqrt{\bar{\alpha}_{t-1}} z'_0 + \sqrt{1 - \bar{\alpha}_{t-1}} \epsilon, \quad \epsilon \sim \mathcal{N}(\mathbf{0}, \mathbf{I}) \\ z_{t-1}^{\text{unknown}} &\sim \text{DDIM}(z'_t, t), \\ z'_{t-1} &= m \odot z_{t-1}^{\text{known}} + (1 - m) \odot z_{t-1}^{\text{unknown}} \end{aligned} \quad (4)$$

We then finish the remaining denoising steps with entire latent codes uniformly.

**Latent Space Harmonization.** Directly applying the inpainting method to blank, unknown regions can lead to disharmonious video content. This is likely because, at a denoising step  $t$ , the content in the unknown regions doesn't fully incorporate the video content in the known regions, creating inconsistencies.

Inspired by FIFO-diffusion [20], our approach leverages content from known regions with reduced noise levels to guide the generation of unknown regions with higher noise

---

**Algorithm 1:** The denoising process of a video diffusion model using Latent-Reframe.

---

**Input:** Initial random noise for 16 frames:  
 $\{z_T^i\}_{i=1}^{16} \sim \mathcal{N}(0, \mathbf{I})$ , Constant parameters of noise scheduler:  $\{\alpha_t\}_{t=1}^T$  and  $\{\bar{\alpha}_t\}_{t=1}^T$ ,  
Pre-trained video diffusion backbone:  $\epsilon_\theta$ ,  
**Input:** diffusion step to perform Latent-Reframe  $t_w$ , point cloud estimation model:  $\mathcal{R}$   
**Output:** Latent code the produced video:  $\{z_0^i\}_{i=1}^{16}$ .

```

1 for  $t = T$  to 1 do
2    $\epsilon \leftarrow \epsilon_\theta(z_t, t)$ 
3   if  $t == t_w$  then
4     Estimated  $z_0 \leftarrow z_t$  using Eq. 1
5     Estimated  $x_0 \leftarrow z_0$  using VAE decoder
6     Time-aware point cloud  $P_{i=1}^{16} \leftarrow \mathcal{R}(x_0)$ 
7     Reframed  $x'_0 \leftarrow (x_0, P_{i=1}^{16})$ 
8     Reframed  $z'_0 \leftarrow x'_0$  using VAE encoder
9     Reframed  $z'_T \leftarrow z'_0$  with reduced noise level
      for the known region
10    for  $t' = T$  to  $t_w$  do
11       $z'_{t-1} \leftarrow z'_t$  using Eq. 4
12  else
13     $z_{t-1} \leftarrow z_t$  using DDIM [33] sampler
14 return  $z_0$ 

```

---

levels, ensuring consistency. Specifically, at the  $t$ -th denoising step, the known regions are assigned noise at the  $(t-3)$  level, while the unknown regions retain noise at the  $t$  level. Ablation studies support the effectiveness of this approach; for further details, see Sec. 4.3.

## 4. Experiment

In this section, we evaluate our method through comparative and ablation experiments. Section 4.1 details the implementation specifics. Section 4.2 compares our approach with other training-based method enabling camera control of video generation methods, providing both quantitative and visual analyses. Section 4.3 examines the impact of individual design components of our method.

### 4.1. Experiment Settings

**Implementation Details.** We choose AnimateDiff [9] as our base model, the generated videos contain 16 frames with spatial resolution  $512 \times 384$ . We employed 25 DDIM denoising steps. For a fair comparison, results from MotionCtrl and CameraCtrl using AnimateDiff are also presented. Point maps were generated using MonST3R [48], and rendering was performed with PyTorch3D [27]. Inference was conducted on a single NVIDIA RTX A5000 GPU, with each sample requiring approximately 3 minutes. Our

method does not require training and can be readily adapted to the inference steps of any other diffusion other models.

**Evaluation Details.** Regarding the evaluation dataset, we utilize 10 prompts mentioned in MotionCtrl and CameraCtrl, combined with 80 poses from the RealEstate10K dataset [50], enabling the generation of 800 videos. Given that both MotionCtrl and CameraCtrl employ implicit poses for embedding, while our method uses explicit poses for rendering, aligning the pose scales, such as translation scale, of videos produced by different methods poses a significant challenge, due to the uncertain scale of the generated scenes. We adjust the camera motion scale for each tested pose manually to ensure that the movements of the camera poses are visually similar. In subsequent quantitative evaluations, we normalize the pose to reduce the impact of scale variations.

We use two types of metrics in the result evaluation: (1) Video quality: We use the Fréchet Inception Distance (FID) [12] and Fréchet Video Distance (FVD) [35] to evaluate the quality of the generated videos. For FVD and FID metric reference, we utilize AnimateDiff with the same prompt to generate 800 videos. Since all comparison methods are built on AnimateDiff, it is expected that the video quality after camera control should degrade minimally and align with that of AnimateDiff. (2) Pose error: In line with CameraCtrl [11], we compute the Rotational Error  $R_{\text{error}}$  and Translational Error  $T_{\text{error}}$  between the estimated pose and the ground truth from RealEstate10K [50]. The formula for Rotational Error is detailed in Eq. 5:

$$R_{\text{error}} = \sum_{j=1}^n \arccos \frac{\text{tr}(\mathbf{R}_{\text{est}}^j \mathbf{R}_{\text{gt}}^{j\top}) - 1}{2}, \quad (5)$$

where  $\mathbf{R}_{\text{est}}^j$  represents estimated rotation matrix and  $\mathbf{R}_{\text{gt}}^j$  represents ground truth rotation matrix for the  $j$ -th frame. The formula for calculating translational error is expressed as follows:

$$T_{\text{error}} = \sum_{j=1}^n \left\| \mathbf{T}_{\text{gt}}^j - \mathbf{T}_{\text{est}}^j \right\|_2, \quad (6)$$

where  $\mathbf{T}_{\text{est}}^j$  and  $\mathbf{T}_{\text{gt}}^j$  respectively denote estimated translation matrix and ground truth translation matrix for  $j$ -th frame. Following ViewCrafter [46], we use DUST3R [38] to estimate the pose. For pose evaluation, we adjust poses to be relative to the first frame, followed by normalization on translation scale.

### 4.2. Main Result

We compare our results with MotionCtrl [40] and CameraCtrl [11], which represent the state-of-the-art methods in camera-controlled video generation. CamTrol [16] achieves camera-controlled image-to-video generation, but it does

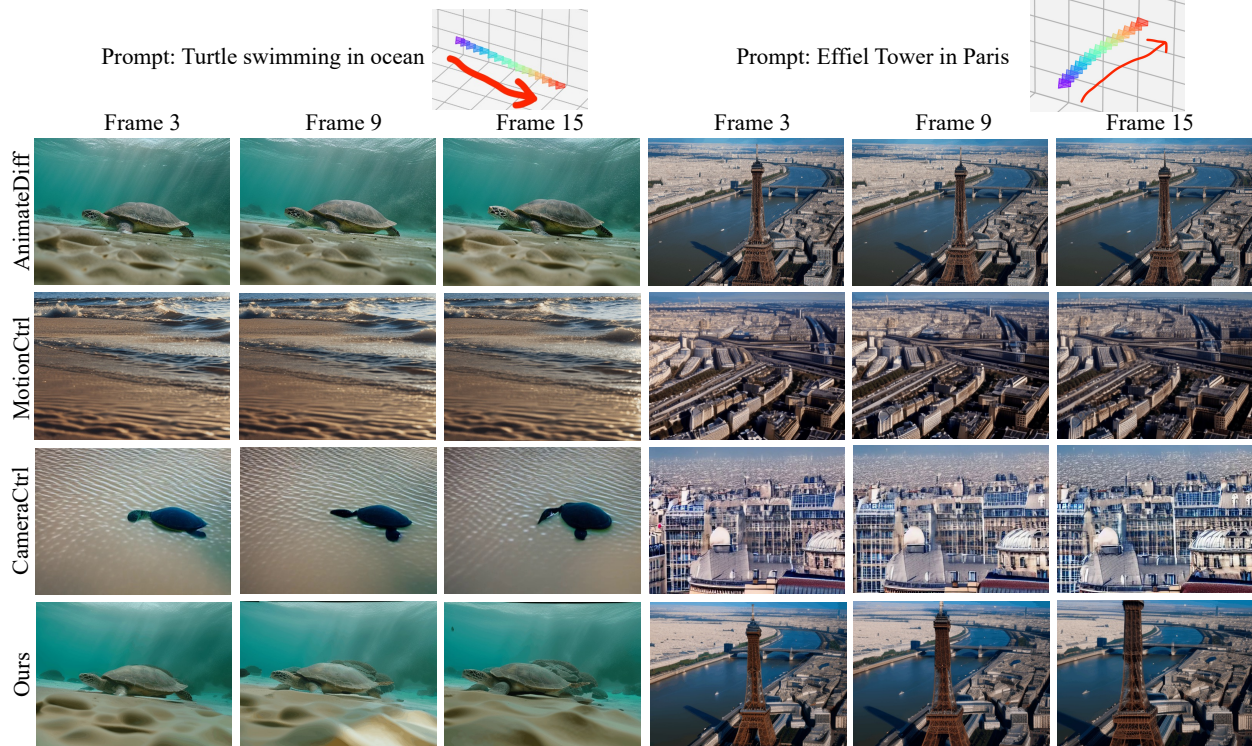


Figure 3. **Visual comparison with state-of-the-art methods.** The proposed Latent-Reframe can generate videos following the given camera trajectory without training. The video quality and the camera pose accuracy are comparable with the compared training-based methods. AnimateDiff is the pre-trained text-to-video diffusion model used by all the compared method. Only Latent-Reframe can keep the learned video distribution of AnimateDiff.

not open source its model and code. Unlike MotionCtrl and CameraCtrl, which embed camera poses and fine-tune the diffusion model on large datasets, our method directly applies to the inference process of existing text-to-video diffusion models. It requires no training.

**Quantitative Evaluation.** As shown in Table 1, our method, without training, is comparable to and even surpasses other methods. In terms of video quality, our method achieves better FID and FVD scores than CameraCtrl. For pose estimation, our method achieves the lowest translation error ( $T_{\text{error}}$ ) and the second lowest rotational error ( $R_{\text{error}}$ ). We attribute the relatively higher rotational error to the reframe-by-inpaint process, which is more effective for modeling translational changes than for rotational changes.

For pose estimation, it is worth noting that each method has video instances where it fails to get pose.

We use the intersection 463 out of 800 samples of successful cases to compare the translational error and rotational error results.

**Visual Analysis.** As illustrated in Fig. 3, while MotionCtrl maintains high video quality, it exhibits instances of semantic misalignment and slow motion. For example, in the left portion of row 2, no turtle appears in the ocean, and

Table 1. **Quantitative Comparisons with training-based methods: MotionCtrl [40] and CameraCtrl [11].** Our Method outperforms CameraCtrl on both video quality and camera pose accuracy. Meanwhile, our method achieves comparable or even better results against MotionCtrl on four evaluated metrics, without training. The best and second best results are marked with **bold** and underline, respectively.

Method	MotionCtrl [40]	CameraCtrl [11]	Ours
FID ↓	<u>63.96</u>	92.40	<b>60.18</b>
FVD ↓	<b>468.29</b>	531.69	<u>509.11</u>
TransErr ↓	<u>7.44</u>	8.39	<b>5.52</b>
RotErr ↓	<b>1.23</b>	2.57	<u>2.29</u>

the waves remain nearly stationary across different frames. Conversely, CameraCtrl demonstrates lower video quality as shown in row 3. Our method achieves both high video quality and effective camera control in video generation without training.

### 4.3. Ablation Study

In the ablation study, we analyze the effect of time-aware point clouds, latent reframing steps, latent space harmoniza-

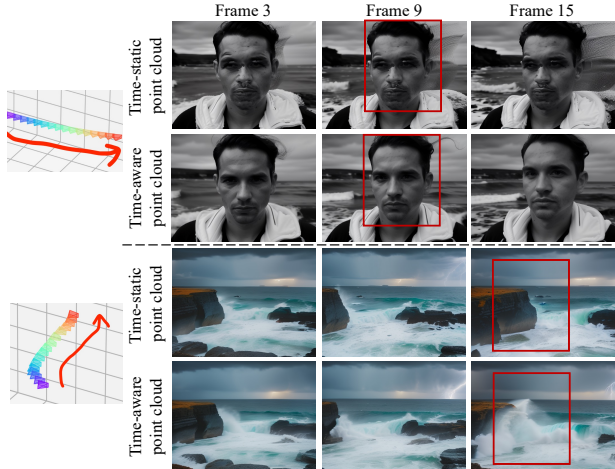


Figure 4. **Comparison between the time-aware and time-static point clouds.** Time-aware point cloud can capture more temporal dynamics of the video, For instance, the motion of the human face (row 1 and 2) and wave (row 3 and 4) are more prominent using time-aware point cloud, both are marked with red bounding boxes.

tion, and different point cloud reconstruction models.

**Time-Aware vs. Static Point Cloud.** We compare two forms of point clouds: a time-static point cloud, which merges point clouds predicted from all images into a single global point cloud and renders the video from the target pose; and a time-aware point cloud, which assigns a temporal scale to the point cloud generated from each frame and considers only the corresponding temporal point cloud during target pose rendering.

As shown in Fig. 4, videos predicted using the single global point cloud appear static. Although minor movements can be observed through the video diffusion model (e.g., the small waves behind the human in the upper rows), the faces of the human remain static and exhibit noise, and the wave movement in the lower rows is minimal. In contrast, videos predicted using the time-aware point cloud retain motion information, such as changes in facial orientation in the upper rows and significant wave movement in the lower rows, while also achieving higher image quality, as highlighted by the red boxes in the figure. This demonstrates that the time-aware point cloud effectively captures and preserves the original dynamic information of the video diffusion model and accommodates corresponding camera control changes.

**Diffusion Step Choice for Latent Reframing.** The latent warping refers to the step in the denoising process of the diffusion model where the latent noisy video is warped to the target poses. We use a total of 25 denoising steps in diffusion model inference, with step 25 corresponding to the state of complete Gaussian noise and step 0 indicating the fully denoised image. We consider three scenarios: per-

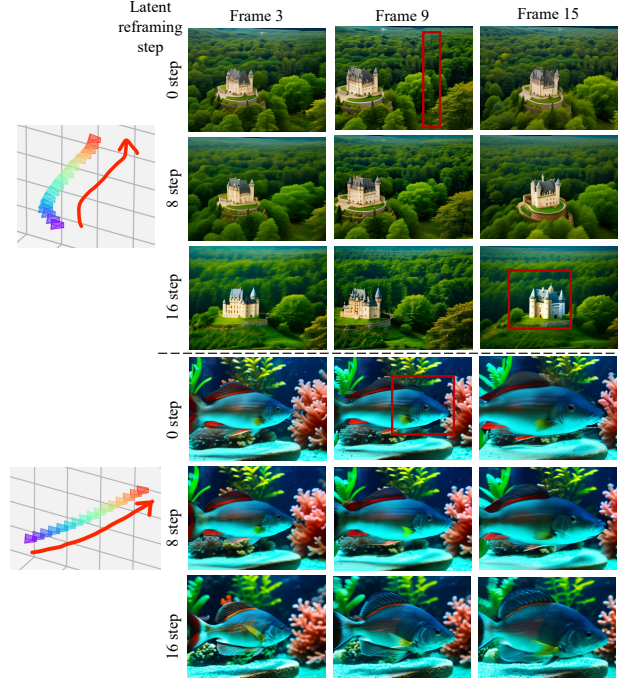


Figure 5. **Comparison between diffusion steps to apply Latent-Reframe.** Using diffusion step 8 out of 25 allows for the reconstruction of high-precision point clouds while leaving enough room for latent space inpainting and harmonization.

forming latent warp at diffusion step 0, 8, and 16.

When the latent warp step is set to 0, the video is fully denoised before pose warping. This approach benefits from the absence of noise, resulting in more accurate pose estimation for the points and images. However, this leads to potential disharmony during the latent inpainting process, as the denoising is applied exclusively to the masked region without integrating the entire image. This issue is evident in Fig. 5, where noticeable strip artifacts appear in the first and fourth rows. Conversely, when the latent warp step is set to 16, the image is at a high noise level, which compromises the accuracy of the reconstructed point cloud. Additionally, the generative capabilities of the video diffusion model overshadow the camera control information provided by the time-aware point cloud in denoising, leading to inconsistencies with the original video content. This is illustrated in the third rows of Fig. 5, where the final columns display content different from previous frames. Setting the latent warp step to 8 strikes a balance, maintaining a moderate noise level that allows for the reconstruction of high-precision point clouds while effectively filling in gaps to match the original video content. This results in harmonious and high-quality videos under new camera poses.

**Noise Reduction Strength for Latent Harmonization.** We investigated the impact of latent harmonization, achieved by reducing noise in known regions, on the gen-

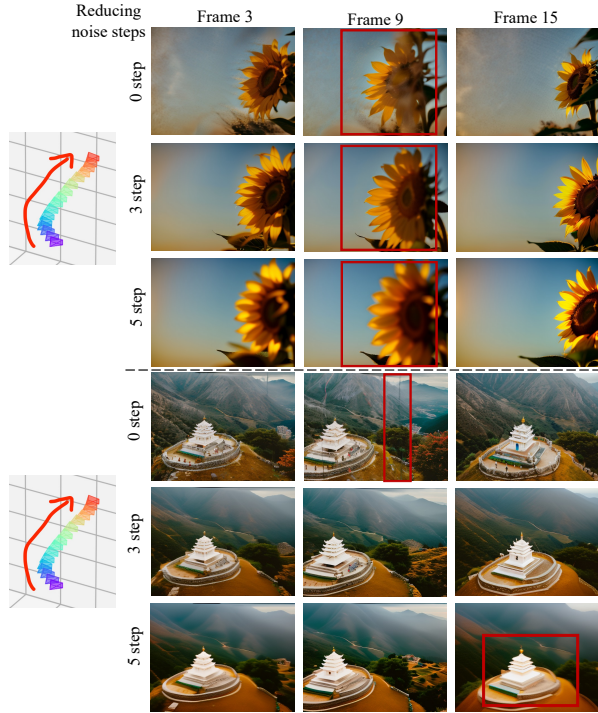


Figure 6. **Comparison between noise reduction steps.** Reducing the noise level of the known region by 3 steps results in videos without significant blurriness or strip artifacts, reaching the best balance.

eration quality of unknown regions. This was measured by decreasing the number of denoising steps, for instance, reducing from 15 to 12 steps represents a reduction of three denoising steps.

We tested reductions of 0, 3, and 5 steps. As shown in Fig. 6, when no noise reduction is applied to the known regions, the final video exhibits noticeable artifacts. In the first row, numerous noise points are observed around the sunflower, while in the fourth row, distinct banding artifacts appear in the middle of the image. This occurs because the denoising process in the known regions does not account for content generation in unknown regions. Conversely, when noise is reduced by 5 steps, the large noise discrepancy between known and unknown regions leads to blurriness, as illustrated in the third and sixth rows. However, reducing noise by 3 steps results in videos without significant blurriness or strip artifacts, achieving the best generation quality. These results indicate that appropriately reducing noise in known regions can significantly enhance the generation of unknown regions, leading to more harmonious videos.

**Choice of Point Cloud Reconstruction Model.** We evaluated three models for extracting time-aware point-cloud information from videos: DUS3R [38], MAS3R [21], and MonST3R [48]. As illustrated in Fig. 7, both MonST3R and DUS3R demonstrated comparable performance, suc-

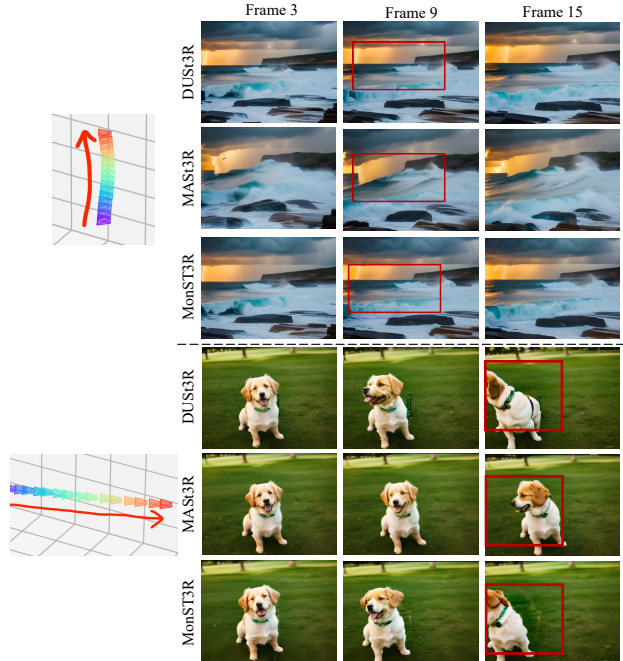


Figure 7. **Comparison between point cloud extraction methods.** MonST3R exhibits better performance in keeping fine details of the video.

cessfully reconstructing high-quality point clouds suitable for rendering. Notably, MonST3R exhibited superior performance in keep fine details of videos. For instance, in the last column of the fourth row, DUS3R produced an elongated neck for the dog, whereas MonST3R maintained a realistic appearance. This improvement can be attributed to MonST3R’s training on dynamic datasets, which enhances its ability to perceive and process dynamic image sequences. Conversely, MAS3R’s reconstructions were less accurate, particularly in pose estimation. This is evident from the significant pose errors in the second row and the failure to reach the target pose in the fifth row.

## 5. Conclusion

This paper presents Latent-Reframe, a method for enabling camera control in video diffusion models without requiring additional training. Latent-Reframe operates during the denoising process with two key steps: a latent reframing step that adjusts the video’s latent code using time-aware point clouds and camera poses, and a latent space rehabilitation step that inpaints occluded regions and harmonizes the latent code for high-quality video generation. Experimental results show that Latent-Reframe achieves comparable or superior camera control precision and video quality compared to training-based methods. This work highlights the effectiveness of leveraging 3D information to enhance 2D video generation.



## References

- [1] Jie An, Songyang Zhang, Harry Yang, Sonal Gupta, Jia-Bin Huang, Jiebo Luo, and Xi Yin. Latent-Shift: Latent Diffusion with Temporal Shift for Efficient Text-to-Video Generation. *arXiv preprint arXiv:2304.08477*, 2023. 2
- [2] Jie An, De Wang, Pengsheng Guo, Jiebo Luo, and Alexander Schwing. On inductive biases that enable generalization of diffusion transformers. *arXiv preprint arXiv:2410.21273*, 2024. 2
- [3] Jie An, Zhengyuan Yang, Jianfeng Wang, Linjie Li, Zicheng Liu, Lijuan Wang, and Jiebo Luo. Bring metric functions into diffusion models. *arXiv preprint arXiv:2401.02414*, 2024. 2
- [4] Andreas Blattmann, Robin Rombach, Huan Ling, Tim Dockhorn, Seung Wook Kim, Sanja Fidler, and Karsten Kreis. Align your latents: High-Resolution Video Synthesis with Latent Diffusion Models. In *CVPR*, 2023. 2
- [5] Haoxin Chen, Menghan Xia, Yingqing He, Yong Zhang, Xiaodong Cun, Shaoshu Yang, Jinbo Xing, Yaofang Liu, Qifeng Chen, Xintao Wang, et al. VideoCrafter1: Open Diffusion Models for High-Quality Video Generation. *arXiv preprint arXiv:2310.19512*, 2023.
- [6] Haoxin Chen, Yong Zhang, Xiaodong Cun, Menghan Xia, Xintao Wang, Chao Weng, and Ying Shan. VideoCrafter2: Overcoming Data Limitations for High-Quality Video Diffusion Models. *arXiv:2401.09047*, 2024. 2
- [7] Zhiwen Fan, Wenyan Cong, Kairun Wen, Kevin Wang, Jian Zhang, Xinghao Ding, Danfei Xu, Boris Ivanovic, Marco Pavone, Georgios Pavlakos, Zhangyang Wang, and Yue Wang. Instantsplat: Unbounded sparse-view pose-free gaussian splatting in 40 seconds, 2024. 2
- [8] Songwei Ge, Seungjun Nah, Guilin Liu, Tyler Poon, Andrew Tao, Bryan Catanzaro, David Jacobs, Jia-Bin Huang, Ming-Yu Liu, and Yogesh Balaji. Preserve Your Own Correlation: A Noise Prior for Video Diffusion Models. In *ICCV*, 2023. 2
- [9] Yuwei Guo, Ceyuan Yang, Anyi Rao, Zhengyang Liang, Yaohui Wang, Yu Qiao, Maneesh Agrawala, Dahua Lin, and Bo Dai. Animatediff: Animate your personalized text-to-image diffusion models without specific tuning. *ICLR*, 2024. 2, 5, 11
- [10] Yuwei Guo, Ceyuan Yang, Anyi Rao, Zhengyang Liang, Yaohui Wang, Yu Qiao, Maneesh Agrawala, Dahua Lin, and Bo Dai. AnimateDiff: Animate Your Personalized Text-to-Image Diffusion Models without Specific Tuning. In *ICLR*, 2024. 2
- [11] Hao He, Yinghao Xu, Yuwei Guo, Gordon Wetzstein, Bo Dai, Hongsheng Li, and Ceyuan Yang. Cameractrl: Enabling camera control for text-to-video generation. *arXiv preprint arXiv:2404.02101*, 2024. 1, 2, 5, 6
- [12] Martin Heusel, Hubert Ramsauer, Thomas Unterthiner, Bernhard Nessler, and Sepp Hochreiter. Gans trained by a two time-scale update rule converge to a local nash equilibrium. *NeurIPS*, 30, 2017. 2, 5
- [13] Jonathan Ho, Ajay Jain, and Pieter Abbeel. Denoising diffusion probabilistic models. *NeurIPS*, 33:6840–6851, 2020. 2
- [14] Jonathan Ho, William Chan, Chitwan Saharia, Jay Whang, Ruiqi Gao, Alexey Gritsenko, Diederik P Kingma, Ben Poole, Mohammad Norouzi, David J Fleet, et al. Imagen Video: High Definition Video Generation with Diffusion Models. *arXiv preprint arXiv:2210.02303*, 2022. 2
- [15] Jonathan Ho, Tim Salimans, Alexey Gritsenko, William Chan, Mohammad Norouzi, and David J Fleet. Video Diffusion Models. In *NeurIPS*, 2022. 2
- [16] Chen Hou, Guoqiang Wei, Yan Zeng, and Zhibo Chen. Training-free camera control for video generation. *arXiv preprint arXiv:2406.10126*, 2024. 2, 4, 5
- [17] Edward J Hu, Yelong Shen, Phillip Wallis, Zeyuan Allen-Zhu, Yuanzhi Li, Shean Wang, Lu Wang, and Weizhu Chen. Lora: Low-rank adaptation of large language models. *arXiv preprint arXiv:2106.09685*, 2021. 2
- [18] Zahra Kadkhodaie and Eero P Simoncelli. Solving linear inverse problems using the prior implicit in a denoiser. *arXiv preprint arXiv:2007.13640*, 2020. 2
- [19] Bernhard Kerbl, Georgios Kopanas, Thomas Leimkühler, and George Drettakis. 3d gaussian splatting for real-time radiance field rendering. *ACM Transactions on Graphics*, 42(4), 2023. 2
- [20] Jihwan Kim, Junoh Kang, Jinyoung Choi, and Bohyung Han. Fifo-diffusion: Generating infinite videos from text without training. In *NeurIPS*, 2024. 2, 4
- [21] Vincent Leroy, Yohann Cabon, and Jerome Revaud. Grounding image matching in 3d with mast3r, 2024. 8
- [22] Fangfu Liu, Wenqiang Sun, Hanyang Wang, Yikai Wang, Haowen Sun, Junliang Ye, Jun Zhang, and Yueqi Duan. Reconx: Reconstruct any scene from sparse views with video diffusion model, 2024. 2
- [23] Andreas Lugmayr, Martin Danelljan, Andres Romero, Fisher Yu, Radu Timofte, and Luc Van Gool. Repaint: Inpainting using denoising diffusion probabilistic models. In *CVPR*, pages 11461–11471, 2022. 4
- [24] Ben Mildenhall, Pratul P. Srinivasan, Matthew Tancik, Jonathan T. Barron, Ravi Ramamoorthi, and Ren Ng. Nerf: Representing scenes as neural radiance fields for view synthesis. In *ECCV*, 2020. 2
- [25] Alexander Quinn Nichol and Pratul P Dhariwal. Improved denoising diffusion probabilistic models. In *ICML*, 2021. 2
- [26] William Peebles and Saining Xie. Scalable diffusion models with transformers. In *ICCV*, pages 4195–4205, 2023. 4
- [27] Nikhila Ravi, Jeremy Reizenstein, David Novotny, Taylor Gordon, Wan-Yen Lo, Justin Johnson, and Georgia Gkioxari. Accelerating 3d deep learning with pytorch3d. *arXiv preprint arXiv:2007.08501*, 2020. 5
- [28] Olaf Ronneberger, Philipp Fischer, and Thomas Brox. U-net: Convolutional networks for biomedical image segmentation. In *MICCAI*, pages 234–241. Springer, 2015. 4
- [29] Yujun Shi, Chuhui Xue, Jun Hao Liew, Jiachun Pan, Han-shu Yan, Wenqing Zhang, Vincent YF Tan, and Song Bai. Dragdiffusion: Harnessing diffusion models for interactive point-based image editing. In *CVPR*, 2024. 2
- [30] Uriel Singer, Adam Polyak, Thomas Hayes, Xi Yin, Jie An, Songyang Zhang, Qiyuan Hu, Harry Yang, Oron Ashual, Oran Gafni, et al. Make-A-Video: Text-to-Video Generation without Text-Video Data. In *ICLR*, 2023. 2

- [31] Brandon Smart, Chuanxia Zheng, Iro Laina, and Victor Adrian Prisacariu. Splatt3r: Zero-shot gaussian splatting from uncalibrated image pairs. *arXiv preprint arXiv:2408.13912*, 2024. [2](#)
- [32] Jascha Sohl-Dickstein, Eric Weiss, Niru Maheswaranathan, and Surya Ganguli. Deep unsupervised learning using nonequilibrium thermodynamics. In *ICML*, pages 2256–2265. PMLR, 2015. [2](#)
- [33] Jiaming Song, Chenlin Meng, and Stefano Ermon. Denoising diffusion implicit models. *arXiv preprint arXiv:2010.02502*, 2020. [3](#), [5](#)
- [34] Yang Song, Jascha Sohl-Dickstein, Diederik P Kingma, Abhishek Kumar, Stefano Ermon, and Ben Poole. Score-based generative modeling through stochastic differential equations. *arXiv preprint arXiv:2011.13456*, 2020. [2](#)
- [35] Thomas Unterthiner, Sjoerd Van Steenkiste, Karol Kurach, Raphael Marinier, Marcin Michalski, and Sylvain Gelly. Towards accurate generative models of video: A new metric & challenges. *arXiv preprint arXiv:1812.01717*, 2018. [2](#), [5](#)
- [36] Ruben Villegas, Mohammad Babaeizadeh, Pieter-Jan Kindermans, Hernan Moraldo, Han Zhang, Mohammad Taghi Saffar, Santiago Castro, Julius Kunze, and Dumitru Erhan. Phenaki: Variable Length Video Generation from Open Domain Textual Description. In *ICLR*, 2023. [2](#)
- [37] Vikram Voleti, Alexia Jolicoeur-Martineau, and Christopher Pal. MCVD-Masked Conditional Video Diffusion for Prediction, Generation, and Interpolation. In *NeurIPS*, 2022. [2](#)
- [38] Shuzhe Wang, Vincent Leroy, Yohann Cabon, Boris Chidlovskii, and Jerome Revaud. Dust3r: Geometric 3d vision made easy. In *CVPR*, 2024. [2](#), [4](#), [5](#), [8](#)
- [39] Xiang Wang, Hangjie Yuan, Shiwei Zhang, Dayou Chen, Junyi Wang, Yingya Zhang, Yujun Shen, Deli Zhao, and Jingren Zhou. VideoComposer: Compositional Video Synthesis with Motion Controllability. In *NeurIPS*, 2023. [2](#)
- [40] Zhouxia Wang, Ziyang Yuan, Xintao Wang, Yaowei Li, Tianshui Chen, Menghan Xia, Ping Luo, and Ying Shan. Motionctrl: A unified and flexible motion controller for video generation. In *ACM SIGGRAPH 2024 Conference Papers*, pages 1–11, 2024. [1](#), [2](#), [5](#), [6](#), [11](#)
- [41] Jay Zhangjie Wu, Yixiao Ge, Xintao Wang, Weixian Lei, Yuchao Gu, Yufei Shi, Wynne Hsu, Ying Shan, Xiaohu Qie, and Mike Zheng Shou. Tune-A-Video: One-Shot Tuning of Image Diffusion Models for Text-to-Video Generation. In *ICCV*, 2023. [2](#)
- [42] DeJia Xu, Weili Nie, Chao Liu, Sifei Liu, Jan Kautz, Zhangyang Wang, and Arash Vahdat. Camco: Camera-controllable 3d-consistent image-to-video generation. *arXiv preprint arXiv:2406.02509*, 2024. [2](#)
- [43] Shiyuan Yang, Liang Hou, Haibin Huang, Chongyang Ma, Pengfei Wan, Di Zhang, Xiaodong Chen, and Jing Liao. Direct-a-video: Customized video generation with user-directed camera movement and object motion. In *ACM SIGGRAPH 2024 Conference Papers*, pages 1–12, 2024. [2](#)
- [44] Botao Ye, Sifei Liu, Haofei Xu, Li Xueting, Marc Pollefeys, Ming-Hsuan Yang, and Peng Songyou. No pose, no problem: Surprisingly simple 3d gaussian splats from sparse unposed images. *arXiv preprint arXiv:2410.24207*, 2024. [2](#)
- [45] Shengming Yin, Chenfei Wu, Jian Liang, Jie Shi, Houqiang Li, Gong Ming, and Nan Duan. Dragnuwa: Fine-grained Control in Video Generation by Integrating Text, Image, and Trajectory. *arXiv preprint arXiv:2308.08089*, 2023. [2](#)
- [46] Wangbo Yu, Jinbo Xing, Li Yuan, Wenbo Hu, Xiaoyu Li, Zhipeng Huang, Xiangjun Gao, Tien-Tsin Wong, Ying Shan, and Yonghong Tian. Viewcrafter: Taming video diffusion models for high-fidelity novel view synthesis. *arXiv preprint arXiv:2409.02048*, 2024. [2](#), [5](#)
- [47] David Junhao Zhang, Roni Paiss, Shiran Zada, Nikhil Karnad, David E Jacobs, Yael Pritch, Inbar Mosseri, Mike Zheng Shou, Neal Wadhwa, and Nataniel Ruiz. Recapture: Generative video camera controls for user-provided videos using masked video fine-tuning. *arXiv preprint arXiv:2411.05003*, 2024. [2](#)
- [48] Junyi Zhang, Charles Herrmann, Junhwa Hur, Varun Jampani, Trevor Darrell, Forrester Cole, Deqing Sun, and Ming-Hsuan Yang. Monst3r: A simple approach for estimating geometry in the presence of motion. *arXiv preprint arXiv:2410.03825*, 2024. [2](#), [4](#), [5](#), [8](#), [11](#)
- [49] Zewei Zhang, Huan Liu, Jun Chen, and Xiangyu Xu. Gooddrag: Towards good practices for drag editing with diffusion models. *arXiv preprint arXiv:2404.07206*, 2024. [2](#)
- [50] Tinghui Zhou, Richard Tucker, John Flynn, Graham Fyffe, and Noah Snavely. Stereo magnification: Learning view synthesis using multiplane images. *arXiv preprint arXiv:1805.09817*, 2018. [4](#), [5](#)

## A. More Results

In this section, we present additional results of Latent-Reframe in camera control for video generation to validate its applicability. These results include both basic camera poses (translational and rotational) and various video styles.

Following MotionCtrl [40], the translational basic camera poses comprise six types: zoom in, zoom out, pan left, pan right, pan up, and pan down, as illustrated in Fig. 10. The rotational basic camera poses include four types: the camera’s own rotations (clockwise and counterclockwise) and the camera’s rotations around an object (rotate clockwise and counterclockwise), as shown in Fig. 9. These results indicate that Latent-Reframe can execute various basic camera controls without requiring any training.

For video generation in different styles, we follow AnimateDiff [9] and apply complex camera pose control across six different video generation styles: FilmVelvia, ToonYou, MajicMix, RcnzCartoon, Lyriel, and Tusun, as shown in Fig. 11. These results demonstrate that Latent-Reframe can effectively manage camera control for video generation across a wide range of styles, highlighting its versatility and suitability.

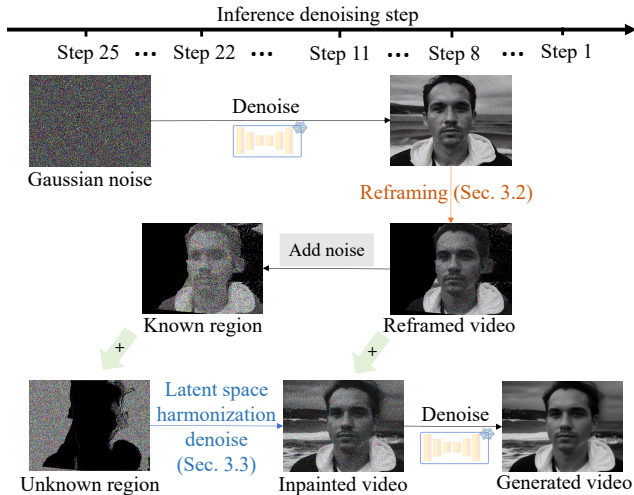


Figure 8. **Denoising time line of Latent-Reframe.** Here, the diffusion step for latent reframing is set to 8, and the noise reduction step is set to 3.

## B. Denoising Process Details

To provide a clearer explanation of the Latent-Reframe inference denoising process, we present the denoising time-line in Fig. 8.

1. The process begins with fully Gaussian noise at the 25<sup>th</sup> step. Denoising is conducted using the video diffusion model until reaching the predetermined latent reframing step, which is step 8.
2. Latent reframing, as described in Sec. 3.2, is then applied to generate the reframed video at the target camera pose.

At this point, holes caused by occlusions are present, and the regions are differentiated into known and unknown regions.

3. The noise addition process starts. As outlined in Sec. 3.3, the noise level in the known region is set to be 3 steps lower than that in the unknown region. For instance, when the unknown region is at the 25<sup>th</sup> denoising step, the known region is at the 22<sup>th</sup> denoising step.
4. Denoising of the unknown region proceeds. At this stage, the input to the denoising network combines unknown and known regions, as described in Eq. 4 of the main paper. The output of the denoising network updates the unknown region for the next step, while the known region for the next step is obtained by adding corresponding noise to the reframed video.
5. When the unknown region reaches the 11<sup>th</sup> denoising step, the known region has already reached the 8<sup>th</sup> step, which is the step for latent reframing. After this, the known region is no longer merged. The denoising process continues normally, updating the entire video until the final step.

## C. Hyperparameter Settings

Tab. 2 further details the parameters employed in Latent-Reframe.

Table 2. **Detail hyperparameter settings.**

Parameter	Value
Video frames	16
Spatial resolution	512×384
DDIM denoising steps	25
Classifier-free guidance scale	7.5
Diffusion step for Latent-Reframe	8
Noise reduction step	3
Point map prediction model	MonST3R [48]
Sliding window size	3
Globally aligned points optimization steps	300

## D. Limitation

While our method effectively enables video generation with camera control without requiring training, it does have certain limitations. For instance, when generating with specific camera poses, especially those involving large movements, can result in visual inconsistencies and artifacts due to extensive unknown regions. Additionally, inaccuracies in the point cloud estimation model and pose estimation can significantly compromise the quality of camera control, leading to errors. Future research will focus on analyzing and mitigating the failure rates associated with these challenging camera poses.

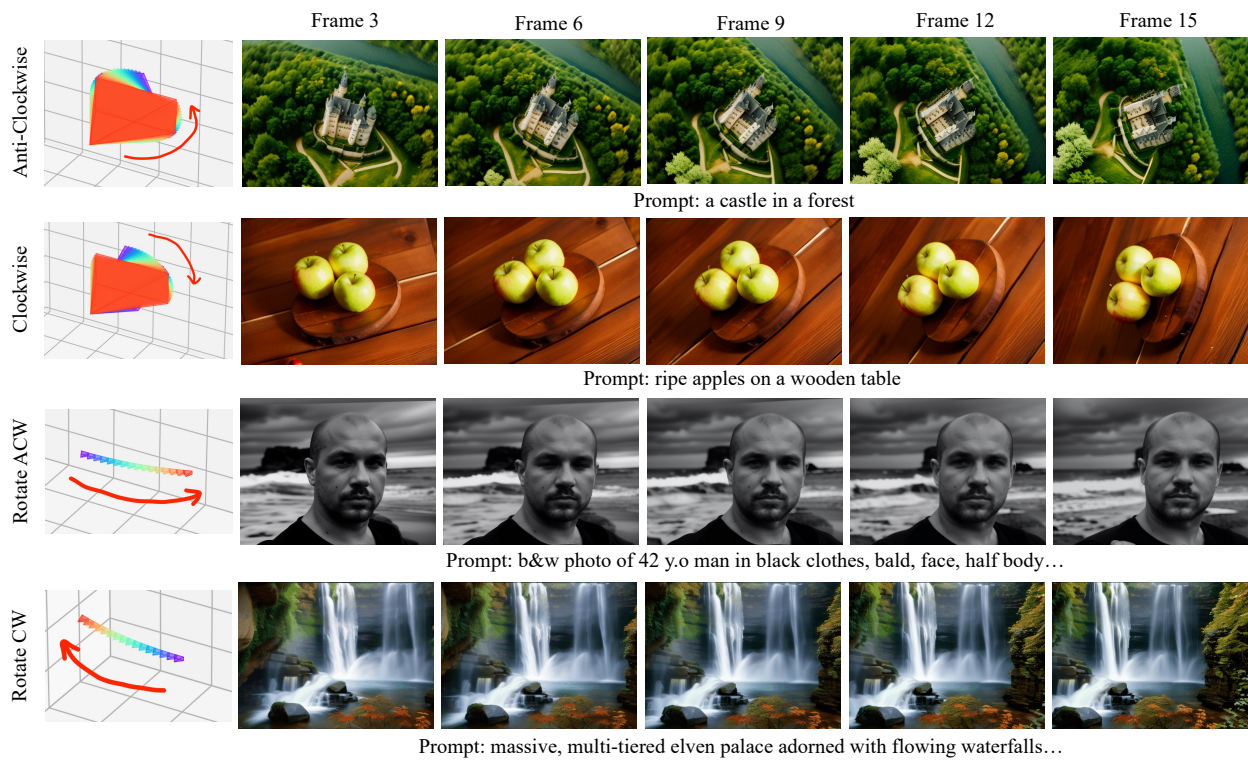


Figure 9. Results of Latent-Reframe camera control for video generation based on rotational basic poses.

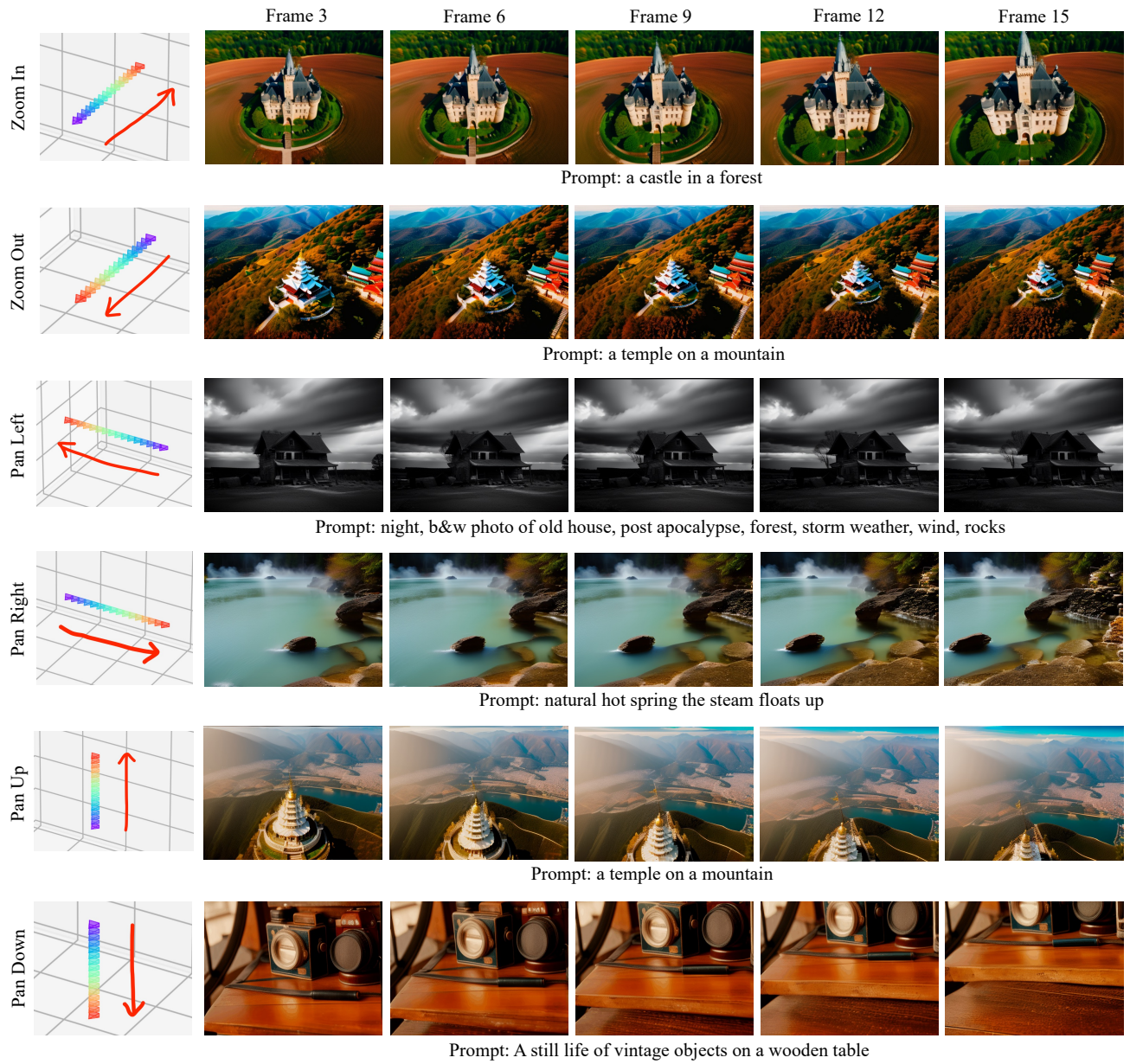


Figure 10. Results of Latent-Reframe camera control for video generation based on translational basic poses.

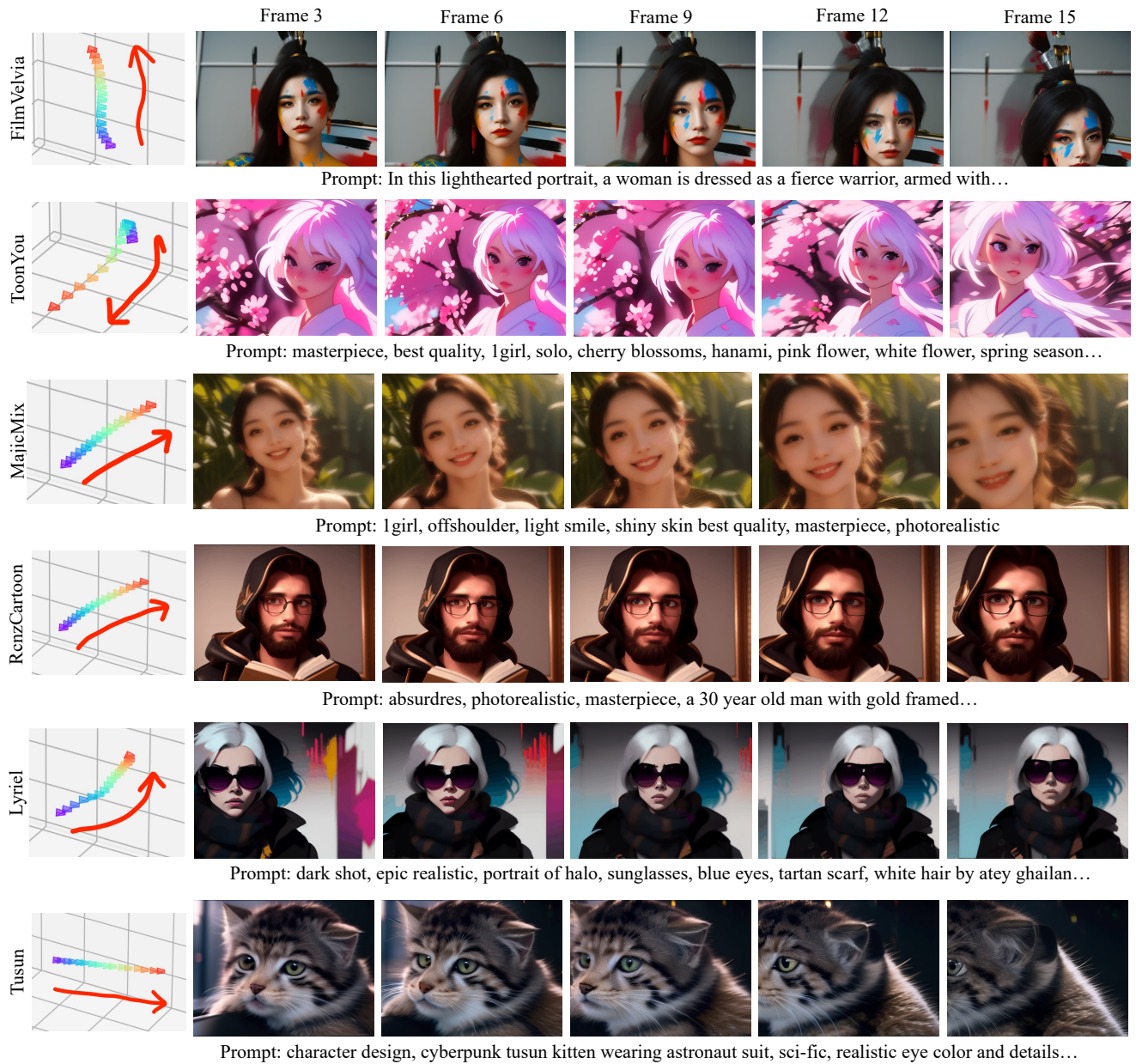


Figure 11. Results of Latent-Reframe complex camera control for various video style.